Unusual growth of the 2023-24 El Niño against the odds of Indo-Atlantic warming

Qihua Peng[1], Shang-Ping Xie[1]*, Ayumu Miyamoto[1], Clara Deser[2], Pengcheng Zhang[1], and Matthew T. Luongo[1]

Affiliations:

[1]Scripps Institution of Oceanography, University of California San Diego, La Jolla, California 92093, USA

[2]National Center for Atmospheric Research, Boulder, CO, USA

Abstract: 2023 was the hottest year on record for the globe as a whole, beating the previous instrumental record by a large margin. 2023 also saw the development of a strong El Niño with worldwide impacts. This El Niño event was unusual for its combination of strong oceanic warming but surprisingly muted atmospheric responses, particularly in terms of the Southern Oscillation and wind anomalies over the tropical Pacific. This discrepancy is perplexing given the historically close coupling of El Niño (EN) and the Southern Oscillation (SO). Using an atmospheric general circulation model, we show that both the extraordinary warming in the Atlantic and Indian Oceans in 2023 and the slow background sea surface temperature trend reduced surface wind response over the tropical Pacific by modulating the Walker circulation. A novel hindcast system we developed captures 87% of June-December averaged El Niño warming even without wind stress feedback after April 2023, primarily driven by the strong buildup of western Pacific heat content during the preceding prolonged La Niña. This explains that the 2023-24 El Niño was highly predictable at long-time leads. These findings challenge traditional ENSO paradigms, revealing that strong El Niño events can arise from oceanic processes alone, independent of the classic positive Bjerknes feedback mechanism. Climate model simulations suggest that such 2023-like El Niño may become more frequent in a warming climate.

A prolonged three-year La Niña took place during 2020-2023[1-4], building up record-breaking ocean heat content (OHC) in the tropical western Pacific (Extended Data Fig. 1f). This La Niña decayed around March 2023, followed by an extreme coastal El Niño off Peru during March-May (Extended Data Fig. 1a)[5]. From June onward, intense sea surface temperature (SST) warming was observed in the eastern equatorial Pacific Ocean (Figs. 1a and 2c; Extended Data Fig. 1), indicating the onset of a basin-scale El Niño. The SST warming signals then propagated westward from the eastern Pacific, with two warming centers[6,7] (Fig. 2c). The eastern Pacific SST anomaly (SSTA) peaked during November-December, with the Niño3 index exceeding +2°C, and then rapidly declined after December 2023, returning to normal levels around April 2024 (Fig. 2c). The average June-January (1) ("1" refers to the year following the peak El Niño) SSTA was +1.88°C, making the 2023-24 El Niño comparable in magnitude to the strong El Niños of 1982-83, 1997-98, and 2015-16 (Figs. 1a-1b;1e-1f). The central-eastern Pacific warming during this event was dominated by interannual variability, and the contribution from long-term SST trends was weak (Extended Data Fig. 2d). The 2023-24 El Niño caused worldwide environmental and societal impacts, such as life-threatening marine and terrestrial heatwaves in 2023[8], record drought and wildfires in the Amazon during 2023-24[9], and torrential rains in the southwestern United States in early 2024[10].

The El Niño development in 2023 was characterized by weak sea level anomalies (SLA) across the equatorial Pacific (Fig. 1a-b), in contrast to the pronounced SLA changes observed for other comparable El Niño events. During April and August, the equatorial Pacific exhibited consistent positive SLA (or subsurface temperature) anomalies, followed by the development of a weak zonal dipole pattern during September to December (Fig. 2c). This behavior contrasts with the pronounced zonal dipole patterns typically linked to a more relaxed slope of the eastward shoaling thermocline seen in other comparable El Niños (Figs. 2c-2d and 2g-2j). The weak SLA (or subsurface temperature) zonal dipole pattern of 2023-24 remained evident with the removal of long-term trends. In 2023, the tropical North Atlantic (0-70°W, equator-30°N) experienced record-breaking SSTAs exceeding 1.2°C (Extended Data Fig. 2a and 2e)[7,11,12]. Typically, tropical Atlantic SSTAs are weak during the development of an El Niño[13-15], making the strong concurrent warming of the eastern Pacific and tropical Atlantic during 2023-24 highly unusual. Pronounced positive SSTAs were also observed in the tropical western Indian Ocean (40°E-70°E, 10°S-10°N), reaching a record-breaking value of +1.2°C at the end of 2023 (Extended Data Fig. 2e). Tropical Indo-Atlantic warming is known to be unfavorable for El Niño development[13,16-20]. During August-November 2023, an extraordinarily strong Indian Ocean Dipole (IOD) developed, with the dipole mode index reaching ~1.6°C, the 4th strongest since 1980. Previous studies have shown that intense cooling in the eastern pole (warming in the western pole) during a positive IOD could induce westerly (or easterly) wind anomalies over the central Pacific, creating favorable (unfavorable) conditions for El Niño[21-23].

It is widely accepted that El Niño arises through positive air-sea feedback between surface wind perturbations and SSTAs[24]. Consequently, stronger Niño 3 warming typically features significantly larger westerly wind anomalies (or a more negative Southern Oscillation Index, SOI), with a correlation of 0.82 (-0.82) (Figs. 1e-1f). However, atmospheric anomalies during the strong 2023-24 El Niño were mysteriously moderate (Figs. 1c)[12]. Specifically, there are sizeable westerly wind, sea level pressure (SLP) and rainfall anomalies near the equator during June 2023-January 2024, but the amplitude of these atmospheric anomalies is much smaller than expected from the composite of similar intensity El Niños (1982-83, 1997-98 and 2015-16) (Figs. 1c-1d and 2a-2b). Figs. 1e-1f show that indeed, the central western Pacific (CWP) zonal wind anomaly averaged in June 2023-January 2024 was only 27% of the expected value based on linear regressions over the period 1982-2023. Extended Data Fig. 1g shows that this percentage varies between -14% and 57% depending on the chosen time window. Consistent with the weaker wind anomalies, the June 2023 to January 2024 averaged SLP difference between the eastern and western Pacific (or SOI) is only 31% of what is expected from the historical regression with fluctuations ranging from 13% to 57% depending on the months analyzed (Extended Data Fig. 1g). The contrast between strong oceanic warming and muted surface wind (or SO) anomalies indicates that the Bjerknes feedback was not well-established during this event. Thus, the conventional positive air-sea feedback mechanisms alone cannot explain the intense ocean warming in the eastern tropical Pacific. Important questions arise regarding the 2023-24 El Niño: What drove the pronounced warming of the eastern equatorial Pacific given the central importance of the zonal wind (e.g., Bjerknes) feedback for El Niño growth? What kept wind anomalies so moderate given that the SSTAs were so strong? Here we investigate these questions using global climate models of varied complexity, including a novel wind-stress prescribed hindcast system. This system allows us to quantify the impacts of wind stress anomalies on the development of this El Niño. Our results show that the buildup of OHC anomalies in the western Pacific as part of the preceding three-year La Niña triggered the 2023-24 El Niño, whereas wind stress anomalies and Bjerknes feedback played a secondary role in the development of this event. These results represent a conceptual advance in understanding ENSO dynamics: El Niño does not necessarily develop through positive air-sea interactions. Even without the Bjerknes feedback (or the SO component), ocean dynamics alone can generate a strong El Niño.

Inter-basin impacts

To investigate the mechanisms moderating the surface wind response during the 2023-24 El Niño, we performed four Atmospheric General Circulation Model (AGCM) experiments (see Materials and Methods; Extended Data Table 1). Forced by observed global SSTs, the control run (aCTRL) captures the overall observed atmospheric anomalies over the tropical Pacific, including the weaker atmospheric responses during the 2023–24 event relative to other comparable El Niños, the easterly anomalies at the beginning of 2023 and the sustained westerly anomalies from June to December (Extended Data Fig. 3a-3b). This underscores the utility of CAM6 in exploring the primary physical mechanisms behind the weak atmospheric response to the 2023 El Niño event. We noted some discrepancies between aCTRL and observations, especially during May-July, when the observed westerly anomalies were more confined to the central Pacific with smaller magnitudes compared to aCTRL (Extended Data Fig. 3a-3b). Some of these discrepancies could arise from high-frequency atmospheric noise, such as westerly wind bursts observed during May-June 2023[7], which cannot be captured by aCTRL.

In 2023, the North Atlantic and western Indian Oceans experienced record-breaking warming (Extended Data Fig. 2a and 2e), which could potentially affect atmospheric anomalies over the tropical Pacific Ocean[16-20]. To explore this possibility, we conducted three AGCM experiments forced by (1) Pacific detrended SSTAs (aPac), (2) Indian-Atlantic detrended SSTAs (aIndAtl), and (3) the background SST trends for 1982-2023 (aTrend) (Extended Data Fig. 2a-2c**)**. This approach allowed us to assess the impacts of Pacific and Indian-Atlantic detrended SSTAs, as well as global SST trends, respectively (see Materials and Methods). Fig. 3b shows that the westerly wind stress anomalies are nearly twice as large in aPac as in aCTRL during the El Niño developing phase, indicating that the Pacific detrended SSTAs alone could drive large surface wind responses in 2023. Importantly, the aIndAtl results indicate that inter-basin impacts from the Atlantic and Indian Oceans induce easterly wind stress anomalies (0.16 N/m^2) over the central Pacific (150°W–170°W, 2°S–2°N), with high consistency across model members (Extended Data Fig. 3c). This leads to a 34% reduction in the surface wind response to El Niño during July–December, broadly consistent with previous studies that strong warming in the tropical Atlantic and Indian Oceans forces a Matsuno-Gill response[25] with an anomalous Walker circulation sinking branch and easterly surface wind anomalies over the tropical eastern

Pacific (Fig. 3e)[13,16-20,26,27]. Recent studies, employing distinct methodologies, have confirmed the importance of pantropical forcing in reducing atmospheric responses during this event[7,12,28].

The long-term SST trend over 1982-2023 played a comparable role in reducing the atmospheric response through modulating the Walker circulation (Figs. 3d and 3f). The SST trend is characterized by relatively large warming in the Indian, Atlantic, and western Pacific Oceans, but muted warming in the eastern tropical Pacific (Extended Data Fig. 2c). The strong warming trend in the Indian and Atlantic oceans induces easterly wind anomalies over the central Pacific through the Matsuno-Gill response[20,26]. In addition, the enhanced zonal SST gradient in the Pacific Ocean accelerates the Walker circulation[29,30], resulting in easterly wind anomalies near the dateline with high inter-member consistency (Extended Data Fig. 3c). From a different perspective, the slower warming trend in the tropical eastern Pacific compared to the overall tropical mean results in slightly negative relative SST trends[31] (Extended Data Fig. 4a), reducing the sensitivity of convection to SSTAs[31-33] and weakening trade winds and SO responses in this region (see Materials and Methods; Extended Data Fig. 4b-d).

The 2023-24 El Niño illustrates that ENSO is not a phenomenon confined to the tropical Pacific basin (Fig. 3) but can be strongly modulated by SST conditions in other tropical basins including long-term trends induced by radiative forcing. This raises an important question of whether an El Niño index (e.g. Nino3.4 SST) is a good measure of global atmospheric anomalies (e.g., the SO). The bottom panels of Fig. 1 show that the answer is yes for a statistically average/typical ENSO event, but individual events require a close look as we did here for the 2023-24 El Niño.

Oceanic dynamics

To reveal the key physical mechanism for the strong oceanic warming of the 2023-24 El Niño, we conduct a mixed layer heat budget analysis based on reanalysis data (Materials and Methods). Extended Data Fig. 5a shows that vertical advection drives the Niño 3 SST warming during June-December. The vertical advection term is dominated by the thermocline feedback ($-\overline{w}T_z'$, TH) term (Extended Data Fig. 5b). Specifically, large subsurface warming was observed in the equatorial Pacific during June-December 2023 (Extended Data Fig. 6c-e), which the mean upwelling pumps into the mixed layer, raising

SST there. Additionally, the reduced upwelling due to the weakened trade winds contributes to the SST warming through Ekman feedback ($-w'\bar{T}_z$, EK) (Extended Data Fig. 5b).

Oceanic General Circulation Models (OGCMs) have been widely used to simulate and investigate SST variability[34,35]. While observed air temperature and specific humidity are often prescribed in calculating surface heat flux, the implied atmospheric thermodynamic forcing of the ocean is physically flawed since these quantities can also be a result of the SSTA and such simulations fail to capture air-sea interactions at the interface[36,37]. Thus, the results of such OGCM experiments might be misleading, especially if SST is the primary focus[37]. Here, we adopt a novel approach to overcoming this issue by forcing a Coupled GCM (CGCM) with observed wind stress but otherwise leaving the model's ocean-atmosphere coupling intact (see Materials and Methods). We conducted sensitivity experiments to investigate the detailed physical processes underlying the 2023-24 event (see details in Materials and Methods; Extended Data Table 2). The control run (CTRL) is a hindcast forced by observed daily wind stress. Fig. 4a shows that the CTRL run successfully reproduces the observed El Niño/La Niña events, with a high correlation of 0.90 between the simulated and observed Niño 3 SST variability. The standard error is 0.14°C, a remarkable achievement enabled by realistic thermodynamic coupling in our "wind-stress overriding" CTRL simulation. Extended Data Fig. 6 further shows that the simulated SSTA, SLA, and equatorial subsurface temperature anomalies for the 2023-24 El Niño agree with observations remarkably well. The good model-observation agreement gives us confidence in using this powerful protocol to uncover the key factors for the 2023-24 El Niño.

Restarting from the initial condition obtained from the CTRL run on 1 April 2023, the InitApr2023 run prescribes observed wind stress but excludes the 31-day running-mean wind stress anomalies from that date onward (see details in Materials and Methods). High-frequency signals within 31-day are retained to minimize model bias[38], but whether these high-frequency signals are included or not turns out not to affect the conclusions of our study (see Materials and Methods; Extended Data Fig. 7). The solutions thus isolate the impacts of the initial conditions on the 2023-24 strong El Niño. The difference, CTRL-InitApr2023 (termed Wind2023), represents the influence of subsequent wind stress anomalies. Fig. 4b shows that the initial conditions on 1 April 2023 play a dominant role in the 2023-24 El Niño event, accounting for 87% of the Niño 3 SST increase averaged in June-December. In contrast, concurrent wind stress anomalies—typically considered crucial for El Niño development—contribute only 13% of the SST warming, with their influence primarily confined to the end of the year, consistent with the emergence of westerly wind anomalies during that period (Fig. 2a). For comparison, we conducted similar experiments (InitAprOther) initialized on April 1 for the three other comparable El Niños of 1982-83, 1997-98, and 2015-16 (see Materials and Methods). Fig. 4c shows that wind stress anomalies (WindOther) contribute nearly all of the Niño 3 SST warming after August. This result aligns with widely accepted ENSO theory[24,39], and stands in stark contrast to the results for the 2023-24 El Niño.

The initial condition for the 2023-24 El Niño is characterized by extraordinarily large positive OHC anomalies (or equivalently SLAs) in the western Pacific (Fig. 4d) from 20˚N to 30˚S. Indeed, the upper 300-m OHC anomaly in the western Pacific at the beginning of 2023 reached its highest value (2.43×10^{22}J) since 1982 (Extended Data Fig. 1f). These large positive OHC anomalies primarily originated from the preceding triple-dip La Niña: Note that positive SLAs persisted in the western Pacific since June 2020 (Extended Data Figs. 8a-8b and 8d-8f). The intensified trade winds (Extended Data Fig. 8c) during 2020-2022 contributed to the buildup of OHC in the western Pacific Ocean (WPAC) through Ekman convergence and downwelling Rossby waves. The strongly tilted thermocline in the east-west direction was balanced by the enhanced easterly trade winds. During March-April 2023, the equatorial trade winds returned to normal as the La Niña decayed (as mimicked by InitApr2023) (Extended Data Fig. 8c and 8h), disrupting the balance between the zonal thermocline gradient and the trade winds and causing the accumulated warm water (or SLAs) in the western Pacific to propagate eastward along the equator as downwelling Kelvin waves (Fig. 4f; Extended Data Fig. 8g-8i; left panels of Extended Data Fig. 9). In the eastern Pacific, SST increased as the mean upwelling transported the subsurface warming into the mixed layer (Extended Data Fig. 10a-10d), consistent with the heat budget results shown above (Extended Data Fig. 5b).

In comparison, a major El Niño is typically preceded by a deepened thermocline in the central equatorial Pacific (Figs. 2f and 4e) in a process known as the "thermocline recharge" [40,41]. The InitAprOther experiment shows that without the wind stress feedback, the recharged thermocline depth anomalies disperse quickly (Fig. 4g; right panels of Extended Data Fig. 9) and the equatorial Pacific Ocean returns to normal in three months at and below the surface (Extended Data Fig. 10e-h). In these comparable El Niño events, the westerly wind anomalies predominantly drive the sustained eastern Pacific warming as part of a marked east-west dipole in subsurface temperature along the mean thermocline as required by the zonal momentum balance (Figs. 4i and 4k). In contrast to this tilt mode of the thermocline depth adjustment to the westerly wind anomalies, the subsurface anomalies are positive across the equatorial Pacific during much of 2023 (Figs. 2g and 4j), characteristic of Kelvin waves that deepen the thermocline. The buildup of OHC in the western Pacific prior to April 2023 that slowly fed the deepened thermocline in the equatorial Pacific (Figs. 4d and 4f) is an interesting topic for further research but beyond the scope of the present study.

The slow ocean dynamic adjustments imply that the 2023-24 El Niño can be predicted at long leads, as OHC carries memory and serves as the major source of predictability[28,42]. Indeed, recent studies noted skillful predictions of the 2023-24 event[28,42-45], but the underlying physical processes and the unique air-sea characteristics of this El Niño have not previously been fully explored through diagnostic analysis and insightful model experiments as done here. Extended Data Fig. 11 presents the forecasts in the North American Multi-Model Ensemble (NMME). With large OHC stored in the western Pacific following the three-year La Niña, most models predicted the El Niño at the beginning of 2023. When initialized on 1 April 2023, the predicted Niño 3.4 (Niño 3) SSTA for December 2023 was 1.64°C (1.73°C), closely matching observations (Extended Data Fig. 11).

Summary and discussion

Statistical analysis of historical events has led to important advances in understanding the coupled dynamics of El Niño and its flavors[46-50]. Our observational analysis has shown that the 2023-24 El Niño was peculiar: the atmospheric responses to the strong equatorial Pacific SSTA were weak compared to those inferred from historical events. This suggests that the Bjerknes feedback was not fully established to promote the growth of this strong El Niño, a surprising result against widely accepted ENSO theory that centers on this coupled feedback mechanism[24,51]. Through novel GCM experiments, our research uncovers major deviations from the current paradigm in ENSO dynamics: we show that even in the absence of tropical air-sea feedbacks (or the SO component), ocean dynamics alone can generate a strong El Niño.

Our AGCM results reveal that strong tropical inter-basin impacts played a vital role in reducing the atmospheric anomalies over the tropical Pacific Ocean during 2023. Specifically, both the record-breaking warmth of the tropical Atlantic and western Indian Oceans in 2023 and the tropical long-term SST trends induced anomalous Walker-circulation subsidence and easterly surface-wind anomalies over the central and eastern Pacific. These influences moderated the tropical atmospheric perturbations associated with the developing El Niño, preventing the full establishment of the Bjerknes feedback during this event. Our results indicate that inter-basin impacts and long-term SST trends were important for the evolution of the 2023-24 El Niño. Without the influence of these pre-existing strong warming in the tropical Atlantic and Indian Oceans, the 2023-24 El Niño would have been amplified considerably, aided by the Bjerknes feedback.

We have developed a novel ocean hindcast system by forcing the ocean component in a CGCM with observed wind stress, which enables us to uncover the key physical processes underlying the strong oceanic warming despite weak Bjerknes feedback during this El Niño. Our experiments using this hindcast system show that the unprecedented buildup of OHC (SLA) in the tropical western Pacific Ocean following a long-lasting La Nina drives SST warming in the eastern equatorial Pacific through downwelling Kelvin waves. As the trade winds returned to their climatological values with the decaying La Niña, downwelling Kelvin waves induced large subsurface warming in the eastern equatorial Pacific Ocean and raised SST through thermocline feedback. Wind stress anomalies, which have been widely considered essential in El Niño dynamics, played a secondary role in the development of the 2023-24 event. With weak wind anomalies during April-October 2023, the equatorial thermocline deepened across the Pacific basin, in contrast with typical El Niños in which the westerly wind anomalies drive an east-west dipole that deepens the thermocline in the east and shoals it in the west. Due to the memory of large OHC anomalies in WPAC, the 2023-24 El Niño seems highly predictable at long lead times[42,43]. The NMME consistently predicted a Niño3.4 warming of ~1^{o}C as early as

January-March 2023 (Extended Data Fig. 11), across the so-called spring predictability barrier[52,53].

We have evaluated possible changes in the occurrences of El Niño like the 2023-24 event in a warming climate using the latest Community Earth System Model version 2 (CESM2). In the 99-member large ensemble (CESM-LENS2), the occurrences of 2023-like El Niño increase markedly from the present to a future warmer climate (Extended Data Fig. 12e; see details in Materials and Methods), due largely to more frequent strong positive SLA events in the WPAC region, with a significant inter-member correlation of 0.63 (Extended Data Fig. 12f). Extended Data Fig. 12g indicates that in WPAC, the sea level response to wind stress increases by ~19% in a warmer climate, driving more frequent strong positive SLA events. To test this hypothesis, we conducted a pair of CESM experiments with identical wind stress but different CO_2 concentrations (details in Materials and Methods). Extended Data Fig. 12h confirms that compared to the present-day climate, the same wind stress variability in a future warmer climate induces stronger WPAC SLA responses, making the western Pacific region more prone to strong positive SLA events, thereby increasing the likelihood of 2023-like El Niños. This increased SLA response to wind stress in a warmer climate may be due to various factors, such as weaker wave damping due to faster phase speeds resulting from enhanced vertical stratification[54] or the nonlinear thermal expansion of seawater[55]. Further research is required to better understand the underlying physical processes.

Methods

Observational datasets and large-ensemble simulation.

We used the monthly NOAA Optimum Interpolation Sea Surface Temperature version 2 dataset (OISSTv2) during 1982-2024[56] and the Global Precipitation Climatology Project (GPCP) during 1979–2024[57]. The ocean temperature, mixed layer depth, currents, and monthly sea level spanning 1980–2024 are obtained from the NCEP Global Ocean Data Assimilation System (GODAS). The daily and monthly surface wind, total rainfall, and air-sea fluxes during 1940-2024 are derived from the ERA5 reanalysis data[58]. All the anomalies in this study are defined relative to the 1982-2022 climatological value.

We analyze outputs from the 99-member CESM-LENS2 to investigate projected changes in the frequency of 2023-like El Niños. Each member differs slightly from others in the initial air temperature field and is driven by historical greenhouse gas and aerosol forcings from 1850 to 2014, followed by the Shared Socioeconomic Pathway 7.0 (SSP3-7.0) emissions scenario from 2015 to 2100. To investigate future ENSO changes, we filtered out low-frequency signals with periods longer than ten years for all variables used. We define 2023-like events as those with a WPAC SLA greater than 4.5 cm in JFM and a Niño 3 SSTA above 0.5°C in November-January (1) (NDJ). Extended Data Fig. 12a-b shows that El Niño events defined this way share similar characteristics with the 2023-24 event, including large western Pacific SLAs during the onset stage, eastward (westward) propagation of SLAs (SSTAs) together with weak equatorial zonal wind stress anomalies during the developing phase. Additionally, the simulated other non-2023-like El Niños (other El Niños excluding 2023-like events) are characterized by weak SLAs in the central Pacific during the onset and strong east-west tilted SLAs with intense westerly wind anomalies during the developing and peak phases, resembling the observed El Niños of 1982-83, 1997-98, and 2015-16 (Extended Data Fig. 12c-d). We track the occurrences of the 2023-like events during 1900-1990 and 2000-2090 to represent the present and future climates, respectively.

AGCM Experiments.

We use the Community Atmosphere Model version 6 (CAM6) to explore the mechanism underlying the muted atmospheric response to the 2023-24 El Niño. The model resolution is 0.9° latitude×1.25° longitude ("f09_f09") with 32 sigma levels in the vertical. We performed four experiments, each comprising 10 ensemble members with slightly different initial conditions. In the aCTRL run, we force CAM6 with observed monthly OISST from January 1982 to December 2023. The aCTRL is radiatively forced by historical forcing until 2014 and then subsequently by the Coupled Model Intercomparison Project phase 6 (CMIP6) Shared Socio-economic Pathway 3-7.0 (SSP370) scenario[59].

Restarting from the initial state from aCTRL on January 2023, we performed two sensitivity experiments forced with the detrended 2023 SSTAs (Extended Data Fig. 2b; Extended Data Table 1) regionally in the Pacific Ocean (aPac; with 5° linear tapering zones outside this region) and the Indian-Atlantic Ocean (aIndAtl) while employing climatological SST during 1982-2022 in other regions. The solution of aPac (aIndAtl) thus isolates the atmospheric response to Pacific (Indian-Atlantic) Ocean regional SSTAs in 2023. Additionally, a third sensitivity experiment, aTrend, was conducted by forcing the model with the global long-term trend component of SSTAs in 2023 (Extended Data Fig. 2c) to assess atmospheric responses to SST trends. The slower warming trend in the tropical eastern Pacific, compared to the overall tropical mean, results in a slightly negative relative SST trend in that region[31]. Because of the weak horizontal temperature gradient in the tropical troposphere, relative SST is a good measure of local atmospheric instability[31-33], exploring the impacts of Pacific relative SST in 2023-24 could offer valuable insights into the physical processes underlying the weak atmospheric response. We thus ran an additional experiment (aPac_RSST), forcing the AGCM with relative SSTAs in the Pacific, while using climatological SSTs in other areas. Extended Data Fig. 4b-4d shows that atmospheric responses in aPac_RSST are weaker compared to aPac. Indeed, a negative relative SST trend indicates that the same level of warming in the eastern Pacific in 2023 triggers weaker convective anomalies compared to the 1982–2022 mean state, thereby reducing trade wind and SO responses.

Mechanisms for long-term trends and interannual anomalies of SST are distinct, the former due to radiative forcing and/or multidecadal variability while the latter due to coupled modes organized in ocean basins (e.g., ENSO and IOD). This justifies our AGCM experiments that isolate interannual SST anomalies of the Pacific from those of the Indo-Atlantic basins (Fig. 3). It is important to note that the SST trends are to first order spatially uniform from the Atlantic to the western Pacific (Extended Data Fig. 2c), consistent with greenhouse radiative forcing. The artificial division of SST trends into geographical ocean basins introduces spurious gradients, resulting in spurious wind responses that mutually offset each other over the western Pacific. We thus did not perform additional sensitivity experiments with basin-specific SST trends.

Wind stress prescribed CGCM experiments.

We used the Geophysical Fluid Dynamics Laboratory coupled model version 2.1[60] to reveal the detailed physical processes underlying the strong oceanic warming for the 2023-24 El Niño. The ocean component is based on the Modular Ocean Model code (MOM4). The ocean model resolution is 1° in latitude and longitude, with a finer meridional resolution of 1/3° near the equator. There are 50 vertical levels, with layer thickness gradually increasing from 10 m near the surface to about 366 m in the deep ocean. The atmosphere and land components are referred to as AM2.1 and LM2.1, with a horizontal resolution of 2° latitude × 2.5° longitude; the atmospheric model has 24 levels in the vertical. The model is forced by the historical radiative forcing of CMIP5 for 1941-2005 and Representative Concentration Pathway 4.5 (RCP4.5) thereafter. In the CTRL run, we prescribe the total surface wind stress over the ocean using observed daily wind stress from ERA5. The model is otherwise fully interactive between the ocean and atmosphere. The CTRL run is integrated forward in time from 1 January 1941 to 31 December 2023, and the last 42 years (1982-2023) are considered in the analysis presented here. The output of CTRL is compared with observations to evaluate the model's performance.

To isolate the effects of initial conditions and wind stress anomalies on the 2023-24 El Niño, we conducted a sensitivity experiment named InitApr2023 (Extended Data Table 2). This experiment was initialized from the CTRL hindcast on April 1, 2023, but with the 31-day running-mean wind stress anomalies removed from that date onward. The high-frequency signals within 31-day were retained to reduce model bias[38]. InitApr2023 was integrated for nine months, to December 31, 2023, thereby isolating the impact of initial conditions on April 1, 2023. Notably, April 1, 2023, was chosen as the initialization date because it coincides with the transition period of when the triple-dip La Niña had just dissipated and the 2023-24 El Niño was about to develop. The difference between the CTRL and InitApr2023 solutions (Wind2023) represents the effects of wind stress anomalies during the El Niño event. Similarly, we conducted sensitivity experiments for three comparable El Niños, initialized on April 1 in the years 1982, 1997, and 2015. The composite of these experiments, referred to as InitAprOther (WindOther), indicates the impacts of initial conditions (wind stress anomalies) on other comparable El Niños. Each of these experiments was performed with three ensemble members. We limited the number of ensemble members to three because the inter-member differences in the tropical regions were found to be quite small for such wind stress-prescribed CGCM experiments. Given that high-frequency wind stress anomalies within the 31-day were retained in both InitApr2023 and InitAprOther, which could potentially influence our conclusions, we designed two additional experiments: InitApr2023_noHighfreq and InitAprOther_noHighfreq. These experiments are identical to InitApr2023 and

InitAprOther, respectively, but exclude the high-frequency wind stress anomalies within 31 days after April 1. Extended Data Fig. 7 shows that the Niño 3 and equatorial SSTAs in the InitApr2023_noHighfreq and InitAprOther_noHighfreq experiments are nearly identical to those in the original experiments, suggesting that the high-frequency wind stress anomalies have minimal impact on our main results.

We emphasize that this wind stress prescribed methodology provides a powerful tool for us to exactly attribute the key dynamic process underlying the 2023-24 El Niño or other tropical climate variability. While other studies have mechanically decoupled the ocean from the atmosphere by overriding wind stress in CGCMs with a simulated field[61-63], very few studies have directly used observed wind stress to drive a CGCM and then investigate the dynamic processes of observed climate variability (e.g., El Niño). The successful application of this method to study the 2023-24 El Niño indicates that this is a powerful tool for quantitatively attributing tropical climate variability and may serve as a better alternative to widely used OGCM experiments.

In addition, we performed two sets of experiments with CESM1.2.2 to evaluate the global warming effect on WPAC sea level variability. The control run, $CTRL_{CESM}$, is a preindustrial simulation with greenhouse gas concentrations and other forcings set to 1850 levels. In this run, surface wind stress is prescribed based on values from a free-running preindustrial simulation[48]. The $Warming_{CESM}$ run is similar to $CTRL_{CESM}$, except that the CO_2 concentration is quadrupled abruptly. It should be noted that in both experiments, the prescribed surface wind stress is identical; the only difference is the CO_2 concentration. The difference between $Warming_{CESM}$ and $CTRL_{CESM}$ could thus be used to investigate how global warming affects the sea level response to wind stress variability. Each experiment runs for 75 years, and the outputs from the last 50 years are analyzed in our study.

Ocean mixed layer heat budget.

Here we employ a mixed layer heat budget[5,64] based on GODAS reanalysis data to investigate the detailed physical processes underlying the 2023-24 El Niño.

$$T_t' = -(\mathrm{u}T_x)' - (\mathrm{v}T_y)' - (\mathrm{w}T_z)' + (\frac{Q_{net}-Q_{pen}}{\rho c_p H})' + R, \quad (1)$$

where T_t' indicates the temperature tendency averaged over the monthly climatological mixed layer depth (H). The first three terms on the right-hand side indicate zonal, meridional, and vertical advection terms, respectively. u, v, and T indicate the mixed layer averaged zonal current, meridional current, and ocean temperature. w is the vertical velocity at the bottom of the mixed layer. The fourth term represents the impacts of thermal forcing. Q_{net} is the net heat flux at the ocean surface, which includes shortwave radiation, longwave radiation, latent heat flux, and sensible heat flux. A positive value of Q_{net} indicates heat flux into the ocean. Q_{pen} is the solar radiation penetration at the bottom of the mixed layer depth. ρ and Cp are the density and specific heat capacity of seawater, respectively; R is the residual term. The vertical advection term [$-(\boldsymbol{wT_z})'$] could be further decomposed into the thermocline feedback ($-\bar{\boldsymbol{w}}\boldsymbol{T_z'}$, TH), the Ekman feedback ($-\boldsymbol{w'}\bar{\boldsymbol{T}}_{\boldsymbol{z}}$, EK), and the nonlinear term ($-\boldsymbol{w'T_z'}$). Here the overbar and prime denote the climatological and anomalous components, respectively.

Data availability

The OISSTv2 dataset is available at https://psl.noaa.gov/data/gridded/data.noaa.oisst.v2.highres.html; ERA5 reanalysis data at https://cds.climate.copernicus.eu/; GPCP at https://psl.noaa.gov/data/gridded/data.gpcp.html; GODAS at https://www.esrl.noaa.gov/psd/data/gridded/data.godas.html; CESM-LENS2 at https://www.cesm.ucar.edu/community-projects/lens2/data-sets.

Code availability

All code supporting the findings of this study is available from the corresponding authors upon request.

Acknowledgements

S.-P.X. was supported by the National Science Foundation (NSF, AGS 1637450). A.M. was supported in part by the Japanese Ministry of Education, Culture, Sports, Science and

Technology programs for the advanced studies of climate change projection (JPMXD0722680395). M.T.L. was supported by NASA FINESST Fellowship 80NSSC22K1528. The National Center for Atmospheric Research (NCAR) is sponsored by the NSF under Cooperative Agreement 1852977. We would like to acknowledge high-performance computing support from the Derecho system (doi:10.5065/qx9a-pg09) provided by the NSF NCAR, sponsored by the NSF.

Author contributions

Q.P. and S.P.X. conceived the study. A.M., Q.P., and M.T.L. performed numerical experiments. Q.P. and A. M. conducted the analysis. Q.P. and S.P.X. drafted the paper. All authors contributed to interpreting the results and improving the manuscript.

Competing interests

The authors declare no competing interests.

Additional information

Correspondence and requests for materials should be addressed to Shang-Ping Xie.

References

1 Fasullo, J. T., Rosenbloom, N. & Buchholz, R. A multiyear tropical Pacific cooling response to recent Australian wildfires in CESM2. *Sci. Adv.* **9**, eadg1213 (2023).

2 Hasan, N. A., Chikamoto, Y. & McPhaden, M. J. The influence of tropical basin interactions on the 2020–2022 double-dip La Niña. *Front. Clim.* **4**, 1001174 (2022).

3 Advances in Atmospheric SciencesIwakiri, T. *et al.* Triple‐Dip La Niña in 2020–23: North Pacific Atmosphere Drives 2nd Year La Niña. *Geophys. Res. Lett.* **50**, e2023GL105763 (2023).

4 Iwakiri, T. *et al.* Triple‐Dip La Niña in 2020–23: North Pacific Atmosphere Drives 2nd Year La Niña. *Geophys. Res. Lett.* **50**, e2023GL105763 (2023).

5 Peng, Q., Xie, S.-P., Passalacqua, G. A., Miyamoto, A. & Deser, C. The 2023 extreme coastal El Niño: Atmospheric and air-sea coupling mechanisms. *Sci. Adv.* **10**, eadk8646 (2024).

6 Geng, X. *et al.* On the spatial double peak of the 2023–2024 El Niño event. **5**, 691 (2024).

7 Hu, R. *et al.* Predicting the 2023/24 El Niño from a multi-scale and global perspective. **5**, 675 (2024).

8 Jiang, N. *et al.* Enhanced risk of record-breaking regional temperatures during the 2023–24 El Niño. *Scientific Reports* **14**, 2521 (2024).

9 Espinoza, J.-C. *et al.* The new record of drought and warmth in the Amazon in 2023 related to regional and global climatic features. *Scientific Reports* **14**, 8107 (2024).
10 L'Heureux, M. L. *et al.* How Well Do Seasonal Climate Anomalies Match Expected El Niño–Southern Oscillation (ENSO) Impacts? *Bull. Am. Meteorol. Soc.* **105**, E1542-E1551 (2024).
11 Zhao, J. *et al.* Lapsed El Niño impact on Atlantic and Northwest Pacific tropical cyclone activity in 2023. *Nat. Commun.* **15**, 6706 (2024).
12 Hong, C. C., Sullivan, A. & Chang, C. C. J. G. R. L. Impact of North Atlantic Tripole and Extratropical North Pacific Extreme SSTs on the 2023/24 El Niño. **51**, e2024GL110639 (2024).
13 Cai, W. *et al.* Pantropical climate interactions. *Science* **363**, eaav4236 (2019).
14 Chang, P., Fang, Y., Saravanan, R., Ji, L. & Seidel, H. The cause of the fragile relationship between the Pacific El Niño and the Atlantic Niño. *Nature* **443**, 324-328 (2006).
15 Latif, M. & Grötzner, A. The equatorial Atlantic oscillation and its response to ENSO. *Clim. Dyn.* **16**, 213-218 (2000).
16 Ding, H., Keenlyside, N. S. & Latif, M. Impact of the equatorial Atlantic on the El Niño southern oscillation. *Clim. Dyn.* **38**, 1965-1972 (2012).
17 Wang, J.-Z. & Wang, C. Joint boost to super El Niño from the Indian and Atlantic Oceans. *J. Clim.* **34**, 4937-4954 (2021).
18 Yu, J.-Y. *et al.* Linking emergence of the central Pacific El Niño to the Atlantic multidecadal oscillation. *J. Clim.* **28**, 651-662 (2015).
19 Kug, J.-S. & Kang, I.-S. Interactive feedback between ENSO and the Indian Ocean. *J. Clim.* **19**, 1784-1801 (2006).
20 Wang, C. Three-ocean interactions and climate variability: a review and perspective. *Clim. Dyn.* **53**, 5119-5136 (2019).
21 Annamalai, H., Xie, S., McCreary, J. & Murtugudde, R. J. J. o. C. Impact of Indian Ocean sea surface temperature on developing El Niño. **18**, 302-319 (2005).
22 Hameed, S. N., Jin, D. & Thilakan, V. J. N. C. A model for super El Niños. **9**, 2528 (2018).
23 Wu, J. *et al.* Boosting effect of strong western pole of the Indian Ocean Dipole on the decay of El Niño events. *npj Climate and Atmospheric Science* **7**, 6 (2024).
24 Bjerknes, J. Atmospheric teleconnections from the equatorial Pacific. *Mon. Weather Rev.* **97**, 163-172 (1969).
25 Gill, A. E. Some simple solutions for heat - induced tropical circulation. *Q. J. Roy. Meteorol. Soc.* **106**, 447-462 (1980).
26 Li, X., Xie, S.-P., Gille, S. T. & Yoo, C. Atlantic-induced pan-tropical climate change over the past three decades. *Nat. Clim. Change* **6**, 275-279 (2016).
27 Wang, L., Yu, J.-Y. & Paek, H. Enhanced biennial variability in the Pacific due to Atlantic capacitor effect. *Nat. Commun.* **8**, 14887 (2017).
28 Zhao, S. *et al.* Explainable El Niño predictability from climate mode interactions. **630**, 891-898 (2024).

29 Toda, M., Kosaka, Y., Miyamoto, A. & Watanabe, M. Walker circulation strengthening driven by sea surface temperature changes outside the tropics. *Nat. Geosci.*, 1-8 (2024).
30 Watanabe, M. *et al.* Possible shift in controls of the tropical Pacific surface warming pattern. *Nature* **630**, 315-324 (2024).
31 L'Heureux, M. L. *et al.* A relative Sea Surface temperature index for classifying ENSO events in a changing climate. **37**, 1197-1211 (2024).
32 Johnson, N. C. & Xie, S.-P. J. N. G. Changes in the sea surface temperature threshold for tropical convection. **3**, 842-845 (2010).
33 Van Oldenborgh, G. J. *et al.* Defining El Niño indices in a warming climate. **16**, 044003 (2021).
34 Peng, Q. *et al.* Eastern Pacific wind effect on the evolution of El Niño: Implications for ENSO diversity. *J. Clim.* **33**, 3197-3212 (2020).
35 Vecchi, G. A. & Harrison, D. The termination of the 1997–98 El Niño. Part I: Mechanisms of oceanic change. *J. Clim.* **19**, 2633-2646 (2006).
36 Deremble, B., Wienders, N. & Dewar, W. CheapAML: A simple, atmospheric boundary layer model for use in ocean-only model calculations. *Mon. Weather Rev.* **141**, 809-821 (2013).
37 Seager, R., Blumenthal, M. B. & Kushnir, Y. An advective atmospheric mixed layer model for ocean modeling purposes: Global simulation of surface heat fluxes. *J. Clim.* **8**, 1951-1964 (1995).
38 Luongo, M. T., Brizuela, N. G., Eisenman, I. & Xie, S. P. Retaining short - term variability reduces mean state biases in wind stress overriding simulations. *Journal of Advances in Modeling Earth Systems* **16**, e2023MS003665 (2024).
39 Hu, S. & Fedorov, A. V. The extreme El Niño of 2015–2016: The role of westerly and easterly wind bursts, and preconditioning by the failed 2014 event. *Clim. Dyn.* **52**, 7339-7357 (2019).
40 Jin, F.-F. An equatorial ocean recharge paradigm for ENSO. Part I: Conceptual model. *J. Atmos. Sci.* **54**, 811-829 (1997).
41 Meinen, C. S. & McPhaden, M. J. Observations of warm water volume changes in the equatorial Pacific and their relationship to El Niño and La Niña. *J. Clim.* **13**, 3551-3559 (2000).
42 Lian, T., Wang, J., Chen, D., Liu, T. & Wang, D. A strong 2023/24 El Niño is staged by tropical Pacific Ocean heat content buildup. *Ocean-land-atmos. res.* **2**, 0011 (2023).
43 Petrova, D., Rodó, X., Koopman, S. J., Tzanov, V. & Cvijanovic, I. J. B. o. t. A. M. S. The 2023/24 El Niño and the Feasibility of Long-Lead ENSO Forecasting. **105**, E1915-E1928 (2024).
44 Petrova, D., Rodó, X., Koopman, S. J., Tzanov, V. & Cvijanovic, I. The 2023/24 El Niño and the Feasibility of Long-Lead ENSO Forecasting. *Bull. Am. Meteorol. Soc.* (2024).
45 Zhang, R.-H., Zhou, L., Gao, C. & Tao, L. J. S. C. E. S. Real-time predictions of the 2023–2024 climate conditions in the tropical Pacific using a purely data-driven Transformer model. 1-18 (2024).

46 Ashok, K., Behera, S. K., Rao, S. A., Weng, H. & Yamagata, T. El Niño Modoki and its possible teleconnection. *Journal of Geophysical Research: Oceans* **112** (2007).

47 Capotondi, A. *et al.* Understanding ENSO diversity. *Bull. Am. Meteorol. Soc.* **96**, 921-938 (2015).

48 Kao, H.-Y. & Yu, J.-Y. Contrasting eastern-Pacific and central-Pacific types of ENSO. *J. Clim.* **22**, 615-632 (2009).

49 Kug, J.-S., Jin, F.-F. & An, S.-I. Two types of El Niño events: cold tongue El Niño and warm pool El Niño. *J. Clim.* **22**, 1499-1515 (2009).

50 Takahashi, K., Montecinos, A., Goubanova, K. & Dewitte, B. ENSO regimes: Reinterpreting the canonical and Modoki El Niño. *Geophys. Res. Lett.* **38** (2011).

51 Wyrtki, K. El Niño—the dynamic response of the equatorial Pacific Oceanto atmospheric forcing. *J. Phys. Oceanogr.* **5**, 572-584 (1975).

52 Duan, W. & Wei, C. The 'spring predictability barrier'for ENSO predictions and its possible mechanism: results from a fully coupled model. *Int. J. Climatol.* **33**, 1280-1292 (2013).

53 Jin, E. K. *et al.* Current status of ENSO prediction skill in coupled ocean–atmosphere models. *Clim. Dyn.* **31**, 647-664 (2008).

54 Zheng, X.-T., Hui, C., Han, Z.-W. & Wu, Y. J. J. o. C. Advanced Peak Phase of ENSO under Global Warming. **37**, 5271-5289 (2024).

55 Widlansky, M. J., Long, X., Schloesser, F. J. C. E. & Environment. Increase in sea level variability with ocean warming associated with the nonlinear thermal expansion of seawater. **1**, 9 (2020).

56 Reynolds, R. W., Rayner, N. A., Smith, T. M., Stokes, D. C. & Wang, W. An improved in situ and satellite SST analysis for climate. *J. Clim.* **15**, 1609-1625 (2002).

57 Adler, R. F. *et al.* The version-2 global precipitation climatology project (GPCP) monthly precipitation analysis (1979–present). *J. Hydrometeorol.* **4**, 1147-1167 (2003).

58 Hersbach, H. *et al.* The ERA5 global reanalysis. *Q. J. Roy. Meteorol. Soc.* **146**, 1999-2049 (2020).

59 Eyring, V. *et al.* Overview of the Coupled Model Intercomparison Project Phase 6 (CMIP6) experimental design and organization. *Geosci. Model Dev.* **9**, 1937-1958 (2016).

60 Delworth, T. L. *et al.* GFDL's CM2 global coupled climate models. Part I: Formulation and simulation characteristics. *J. Clim.* **19**, 643-674 (2006).

61 Larson, S. M. & Kirtman, B. P. Revisiting ENSO coupled instability theory and SST error growth in a fully coupled model. *J. Clim.* **28**, 4724-4742 (2015).

62 Luongo, M. T., Xie, S.-P. & Eisenman, I. Buoyancy forcing dominates the cross-equatorial ocean heat transport response to Northern Hemisphere extratropical cooling. *J. Clim.* **35**, 6671-6690 (2022).

63 Larson, S. M., Buckley, M. W. & Clement, A. C. Extracting the buoyancy-driven Atlantic meridional overturning circulation. *J. Clim.* **33**, 4697-4714 (2020).

64 An, S.-I. & Jin, F.-F. Nonlinearity and asymmetry of ENSO. *J. Clim.* **17**, 2399-2412 (2004).

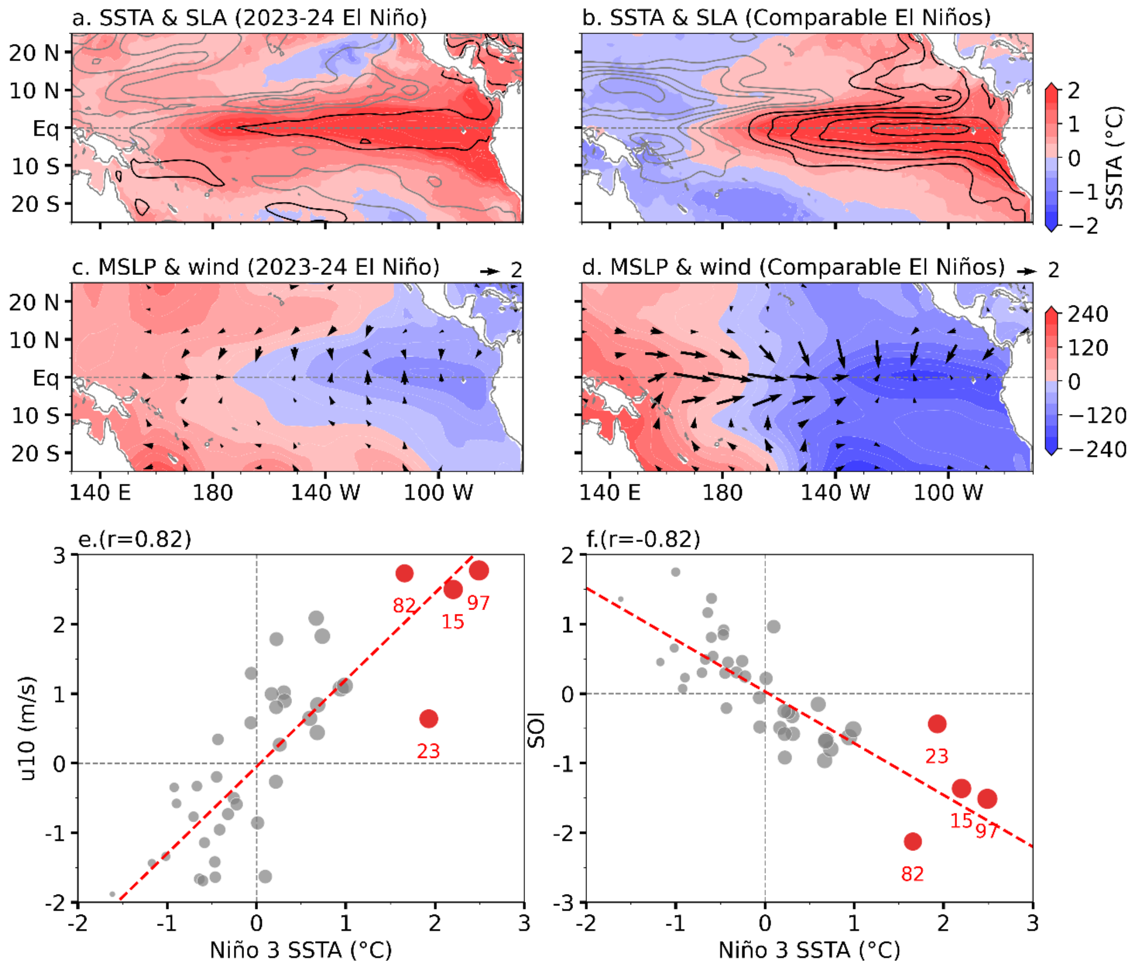

Fig. 1 | Climate states for the 2023-24 El Niño. June-January (1) observed SSTA (℃, color shading) and SLA (contours with an interval of 0.04 m; positive black and negative grey) for (a) the 2023/24 El Niño and (b) the other comparable El Niño composite. (c)-(d) Same as (a)-(b) except for the mean Sea Level Pressure (MSLP; color shading) and 10-m wind anomalies (m/s, vectors). Scatter plot for June-January (1) (the numeral 1 refers to the second year of El Niño) Niño 3 averaged SSTAs (℃) versus concurrent (e) Central-Western Pacific (CWP; 140˚E–160˚W, 5˚S–5˚N) 10-m zonal wind anomalies and (f) SOI. The dot size represents the amplitude of Niño 3 SSTAs.

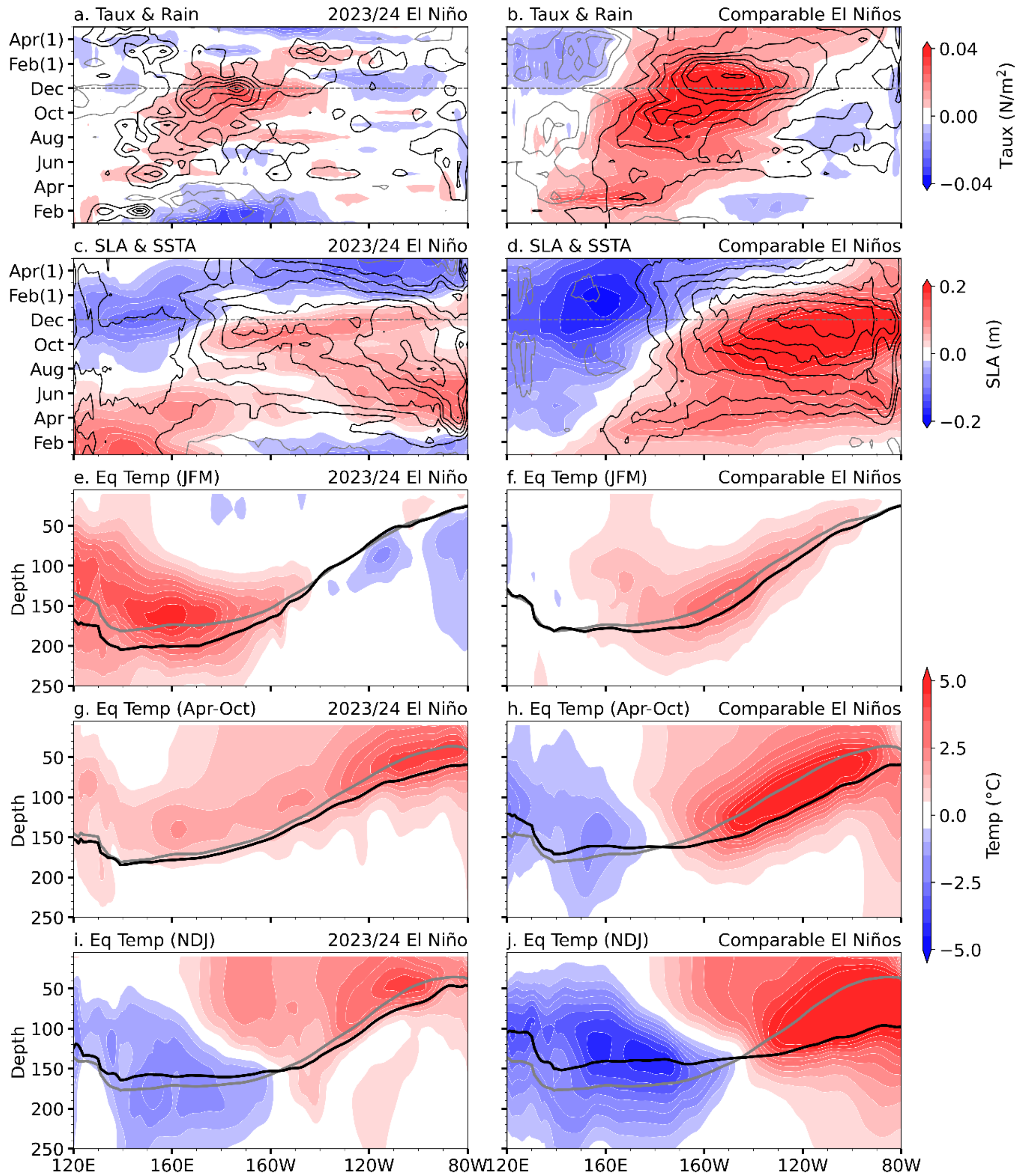

Fig. 2 | Evolution of the 2023-24 El Niño and the composite El Niño based on comparable events (1982-83, 1997-98 and 2015-16). Hovmöller diagram of equatorial (a) zonal wind stress (color shading; N/m^2) and rainfall anomalies (contours with an interval of 1.5 mm/day; positive black and negative grey; amplitude smaller than 3 mm/day omitted) and (c) SLA (m, color shading) and SSTA (°C, contours with an interval of 0.5 °C; positive black and negative gray) for the 2023-24 El Niño. The (e) January-March (JFM), (g) April-October, and (i) November-January (1) (NDJ) averaged equatorial ocean temperature anomalies (°C, color shading) for the 2023-24 El Niño. The black (grey) line represents the 2023 (climatological) 20 °C isotherm. The right panels are similar to the left panels but for the El Niño composite based on comparable events. All anomalies are meridionally averaged over 2˚S–2˚N.

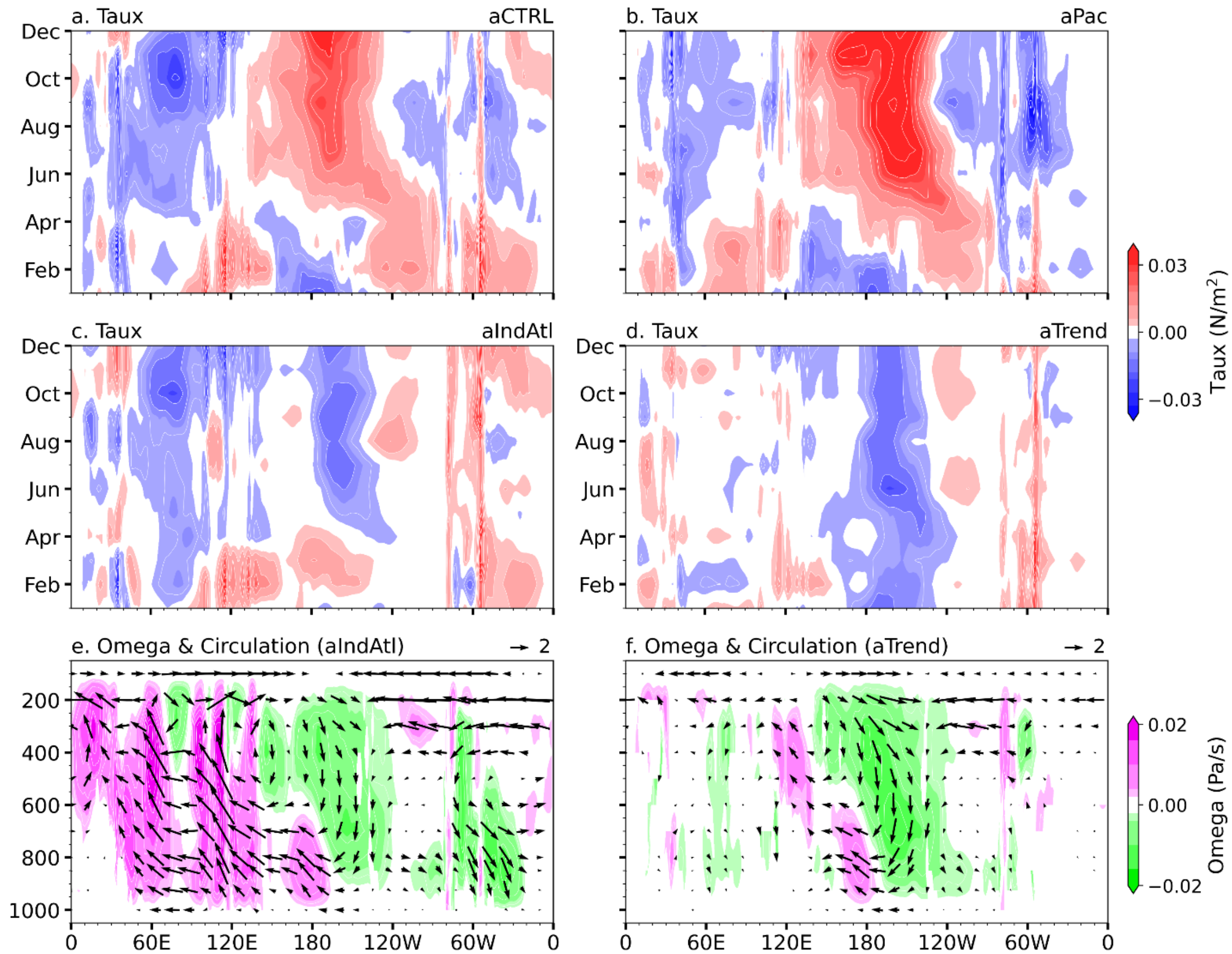

Fig. 3 | Atmospheric response from the AGCM experiments. Hovmöller diagram of equatorial zonal wind stress anomalies (color shading; N/m^2) from (a) aCTRL, (b) aPac, (c) aIndAtl, and (d) aTrend runs (see Materials and Methods). The associated June-December averaged vertical velocity (Pa/s, color shading; a positive value indicates ascending motions) and Walker circulation changes (vectors, m/s; the vertical velocity is magnified by a factor of 200 for visualization purposes) from (e) aIndAtl and (f) aTrend.

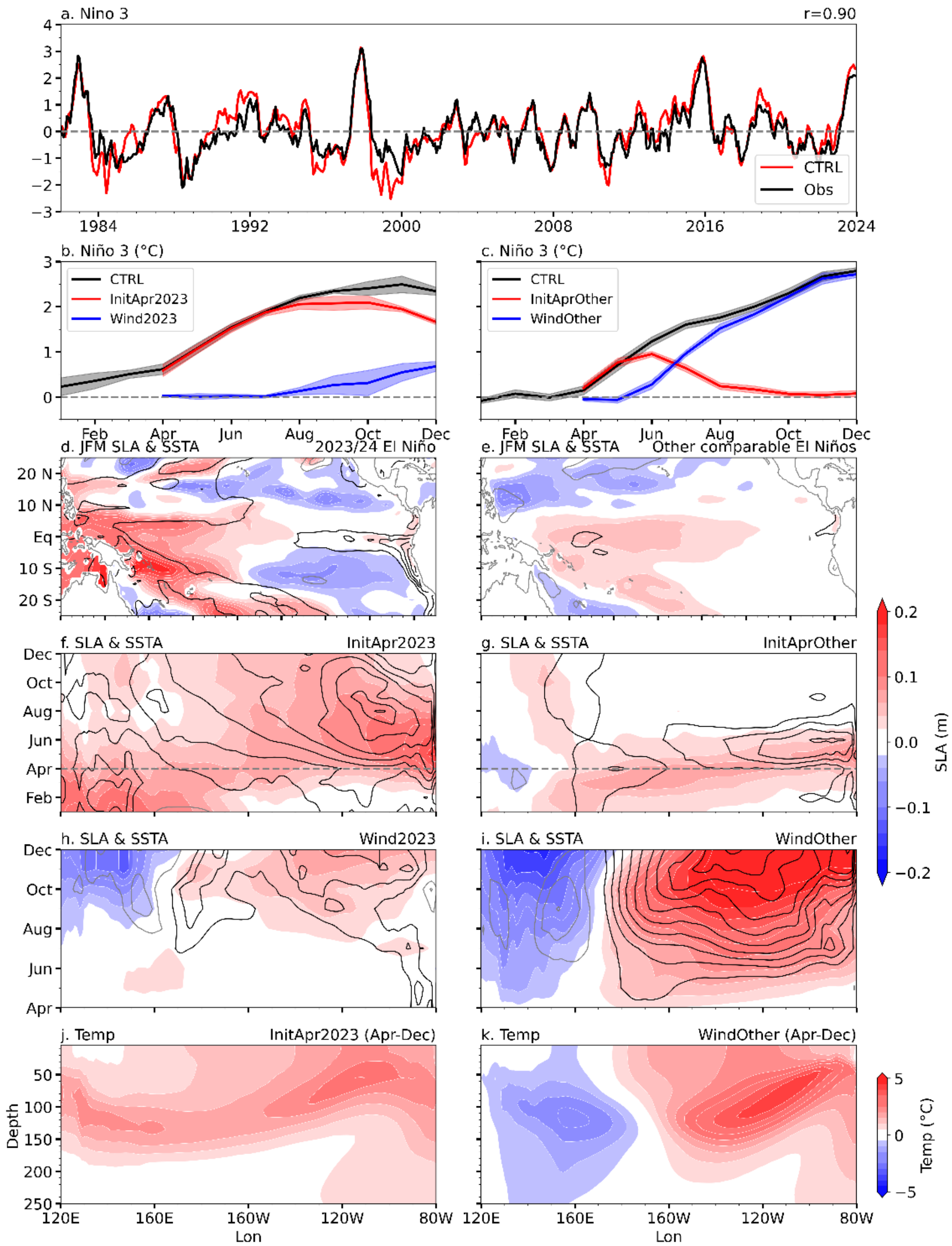

Fig. 4 | The impacts of ocean initial conditions and wind stress anomalies on the 2023-24 El Niño and the other three comparable El Niños. (a) Simulated (CTRL) and observed (Obs) Niño 3 SSTA (℃) during January1982-December 2023. (b) Simulated Niño 3 SSTAs from the CTRL, InitApr2023, and their difference (Wind2023). (d) Horizontal distribution of SLA (m, color shading) and SSTA (℃, contours) averaged in JFM 2023 from the CTRL run, which generally represents the initial conditions for InitApr2023. Hovmöller diagram of equatorial SLA (m, color shading) and SSTA (contours) from the (f) InitApr2023 and (h) Wind2023 experiment. Contours are shown at 0.5°C intervals, with positive black and negative gray. (e), (g), and (i) are similar to (d), (f), and (h) but for the composite of the other comparable El Niños (see Materials and Methods). Longitude-depth diagram of April-December equatorial ocean temperature anomalies (℃, color shading) from (j) InitApr2023 and (k) WindOther, respectively.